A theoretical analysis of the atmospheric gravity wave that connects the thermosphere and the troposphere

Misako HAGIWARA[a] and Hiroshi L. TANAKA[b*]

Abstract

The purpose of this study is to theoretically analyze how atmospheric gravity waves (AGWs) generated in the thermosphere propagate down to the troposphere, using an expansion in three-dimensional normal mode functions (3-D NMF). The 3-D NMF is an orthonormal expansion basis for observed data. Using linear primitive equations in a spherical coordinate system, we set the initial variables of zonal wind, meridional wind, and geopotential height perturbations. With the initial state of waves and performing analytical time integration up to 24 hours, it is possible to express the theoretical wave propagations according to the linear theory. When the impact of geopotential height is placed at high latitudes and high altitudes assuming a solar activity change of aurora oval, we find that the impact can propagate downward to the troposphere as attenuating gravity waves. It is found that the wave propagations and reflections at the surface create an anti-node of geopotential at the bottom of the atmosphere corresponding to the vertical width of the initial state of the impact. On the other hand, standing waves in temperature create a node at the ground surface. The characteristic vertical structure near the ground surface comes from the lower boundary condition of the vertical structure functions. Due to the standing waves generated in the lower troposphere, the atmospheric stability is altered by the passage of the gravity waves in the meridional direction. Thus, it is considered that the gravity waves can affect the development of cyclones by changing the stability parameters. Waves propagating from higher altitudes reach the troposphere, but the amplitude of AGWs has been reduced from about 1,000 to 10,000 times. Since the temperature response in the thermosphere due to the aurora oval is estimated as hundreds to a thousand K, there is a response of 0.01 to 0.1 K when the waves reach to the troposphere.

[a] Graduate School of Life and Environmental Sciences, University of Tsukuba, Tsukuba, Japan
[b] Center for Computational Sciences, University of Tsukuba
[*] Corresponding author: Hiroshi L. Tanaka, Center for Computational Sciences, University of Tsukuba, Tsukuba, Ibaraki 305-8577, Japan.
Email: tanaka@ccs.tsukuba.ac.jp
Tel: +81-29-853-6482   Fax: +81-29-853-6489

1. Introduction

Climate change over the past long period can be partly explained by Milankovitch cycle and solar activity. The seasonal variation of quantity of solar radiation induced by the Milankovitch cycle can show the variation of Asian summer monsoon during the Medieval warm period and Little Ice Age (Kamae et al., 2017). In the meantime, solar activity is determined by the increase or decrease of the number of sunspots, which has an inverse correlation with galactic cosmic rays. It has been studied since the 1950s that galactic cosmic rays can penetrate and affect the earth's atmosphere (Ney, 1959). In particular, Svensmark and Friis-Christensen (1997) has proposed a theory that there is a relationship between cosmic rays and changes in cloud amount, but there are still many discussions (Gray et al., 2010; Pierce and Adams, 2009; Kristjánsson et al., 2002).

When the high-speed solar wind associated with solar activity reaches the Earth, geomagnetic activity increases, causing phenomena such as magnetic storms and aurora. They sometimes interfere with satellites and communication equipment, therefore more accurate space weather forecast becomes important for monitoring and observing space and predicting the effects on the Earth. Wilcox et al. (1973) investigated a link between the solar magnetic sector structure and the pressure troughs observed at 300 hPa in the Northern Hemisphere during winter, indicated that the average area of large vorticity over several days is reduced when the sector boundary passes through the Earth by the solar wind, i.e., the pressure troughs become smaller. Fujita and Tanaka (2007) statistically showed that the Arctic Oscillation Index has a positive structure during maximum solar and geomagnetic activity, and that geomagnetic activity has more influence on the Arctic Oscillation. As a process connecting geomagnetic with tropospheric activity, it has been suggested that the stratospheric ozone is reduced by the influx of high-energy particles into the polar region, which increases the temperature gradient between the polar and equatorial stratosphere and enhances the Arctic Oscillation (Kodera and

Kuroda, 2002).

In addition, an aurora contributes to the geomagnetic disturbance. In a study related to aurora and atmospheric phenomena, Prikryl et al. (2003) suggested that atmospheric gravity waves (AGWs) generated by auroral jet currents caused fluctuation of mid-latitude low-level clouds at the mesoscale. Furthermore, Prikryl et al. (2016; 2018) found that the rapid development of low pressure system in both the Northern and Southern Hemispheres is observed in few days after the arrival of high-speed solar winds to the Earth. As this factor, they pointed out that AGWs generated in the lower thermosphere at high latitudes by the aurora played an important role.

In the troposphere, AGWs are known to be excited by topography, and its impacts have been simulated by Vadas et al. (2003). When AGWs generated at the lower atmosphere propagate upward to the middle atmosphere, the amplitude becomes larger in the middle atmosphere where the density becomes lower, and they cannot maintain their structure. At this time, they deposit the angular momentum that they have transported and drive the meridional circulation. This effect has been incorporated to the General Circulation Model of the Atmosphere (GCM) and has contributed to improved forecast accuracy (Tsuda, 2014). The atmospheric general circulation in the mesosphere was analyzed using the potential vorticity devised by Sato et al. (2018), and showed that the momentum balance in the mesosphere-lower thermosphere region is due not only to Rossby waves and gravity waves (GWs, which are the waves caused by a variety of factors unlike AGWs) generated in the mesosphere, but also to those in the troposphere. Furthermore, Yasui et al. (2018) suggested that GWs forcing generated from the lower atmosphere causes barotropic/baroclinic instabilities and shear instability to produce Rossby and GWs in the mesosphere, respectively, and that the formation and dissipation of these waves play important roles in the mesosphere and lower thermosphere. In recent years, wind speed and temperature in the upper atmosphere have been observed by sodium lidars, meteor radars, WINDII (Scanning Michelson Interferometer for Wind Measurement), and the Program of the Antarctic Syowa MST/IS Radar (PANSY) at Showa Station in Antarctica, which can capture the AGWs. Tsuda (2011) showed that zonal-mean winds with speeds as high as 100 m/s in the mid-atmosphere weaken or reverse direction at an altitude of 80 km. This phenomenon can also be confirmed by a simulation using a quasi-one-dimensional model of the mid-atmosphere general circulation that takes into account the interaction of the internal gravity waves described in Matsuno (1982); however, a frictional effect of the atmospheric waves in-

cluding AGWs is needed to understand this phenomenon. Observational studies of AGWs show that they are excited by a variety of mechanisms and always occur over the globe.

In the thermosphere, observations of traveling ionospheric disturbances (TIDs) allow to see atmospheric gravity waves in the ionosphere and thermosphere. According to Xu et al. (2013), satellite observations by TIMED (Thermosphere, Ionosphere, Mesosphere Energetics and Dynamics) and MIPAS (Michelson Interferometer for Passive Atmospheric Sounding) show that the impact of auroral heating on the neutral atmosphere reaches about 105 km. They also argue that below the mesosphere the phase of temperature perturbation does not coincide with the temperature change caused by auroral heating and that other processes may cause temperature perturbations. A simulation by Idenden (1998) for a travelling atmospheric disturbance (TAD, almost synonymous with TID) during the expansion of the auroral oval has an initial setting of neutral atmospheric temperature of 1060 K from the upper thermosphere to about 300 km altitude. This simulation shows that the rising temperature region alters due to the equatorial expansion and energy input changes, which excites a TAD. It has also been suggested that vertical winds are important not only for heat redistribution but also for the composition of the thermosphere and the change of ionospheric density. Richmond and Matsushita (1975) solved equations and performed time integration that included the effects of the ionospheric atmosphere. It was found that atmospheric disturbances with wind speeds of 200 m/s and temperature fluctuations of 100 K were observed at mid-latitudes, using disturbances in the thermosphere and polar regions as sources, and that the AGWs propagated at a velocity of about 750 m/s over a distance of 10,000 km. It is the Lorentz force and Joule heat that provide energy for the AGWs (Tanaka, 1979), and their contributions have been quantitatively analyzed (Chimonas and Hines, 1970; Crowley and Williams, 1987). In addition, the analysis by Richmond (1978) revealed that the direction of propagation of AGWs in the thermosphere depends on their velocity. Francis (1974) showed that the auroral jet current at 120 km altitude, influenced by viscous dissipation, temperature stratification, and surface reflections, caused AGWs. Francis (1975) suggested that a discrete spectrum in the upper atmosphere and a continuous spectrum of freely propagating internal waves were involved as the fundamental mechanism about the response of aurora to the atmosphere, consistent with observations of mid-latitude TIDs. Therefore, the propagation of AGWs generated by the aurora has been studied both observationally and the-

oretically. Furthermore, Prikryl et al. (2018) simulated the propagation of AGWs using the Transfer Function Model (TFM) (Mayr et al., 1990; Mayr et al., 2013) and found that the waves generated and propagating in the thermosphere are greatly reduced in amplitude but increased when reflected in the upper troposphere. The results suggest that in a symmetric unstable atmosphere occurring in a baroclinic fluid in the troposphere, only a slight lifting of the air mass can induce slantwise convection that forms a precipitation zone. Symmetric instability has been attributed to the enhancement of rain and snow near the front associated with mesoscale precipitation zones and extratropical cyclones (Ogura, 1997); the energy supplied by latent heat release is considered as one of factors of it. However, there are few theoretical studies that show the AGWs reaching the troposphere.

Therefore, in this study, we show the theoretical analysis of how AGWs generated in the thermosphere can propagate to the troposphere, using 3-D normal mode functions (NMF) on a sphere. Expansion in the 3-D NMF is a technique to represent the spectrum of the observational data. Linear differential equations in terms of perturbations of zonal wind, meridional wind, and geopotential height are obtained from the primitive equations in a spherical-coordinate system. The vertical and horizontal structural equations can be derived by separating variables in the vertical and horizontal directions. In this study, the vertical structure function and the horizontal structure function, which are the analytical solutions of each equation, are combined to expand the variables. The purpose of this study is to theoretically investigate the propagation of AGWs generated in the lower thermosphere, using the expansion in the 3D NMF. The method of this study is described in Section 2. Section 3 presents the results of the analysis. Finally, summary and discussion of this study is given in Section 4.

2. Methods

The basic theory of the 3-D NMF used in this study is described in Tanaka (1985). Assuming the basic state to be adiabatic and no friction in the atmosphere at rest, the primitive equations can be expressed as a vector form as

$$M \frac{\partial U}{\partial \tau} + LU = 0, \tag{1}$$

where, U is a state variable vector composed by perturbations of zonal wind u, meridional wind v, and geopotential ϕ.

$$U = \begin{pmatrix} u \\ v \\ \phi \end{pmatrix}, \tag{2}$$

M and L are differential operator in the vertical and horizontal directions, respectively. τ is dimensionless time. Refer to Tanaka (1985) for the symbols and differential operators.

The 3-D NMF $\Pi_{nlm}(\lambda, \theta, \sigma)$ is obtained by combining the vertical structure function and the horizontal structure function of zonal wavenumbers n, meridional index l, and vertical index m:

$$\Pi_{nlm}(\lambda,\theta,\sigma) = G_m(\sigma) H_{nlm}(\lambda,\theta), \tag{3}$$

where λ and θ are longitude and latitude, respectively. σ represents the non-dimensional pressure p scaled by a constant surface pressure p_s.

The vertical structure function can be obtained by setting the following boundary conditions:

$$\frac{\partial G_m}{\partial \sigma} = 0, \quad \text{at} \quad \sigma = \epsilon > 0, \tag{4}$$

$$\frac{\partial G_m}{\partial \sigma} + \alpha G_m = 0, \quad \text{at} \quad \sigma = 1, \tag{5}$$

where ϵ is the dimensionless pressure at the upper end of the atmosphere and α is the ratio of the static stability parameter γ to the isobaric surface mean temperature T_0. In this study, in order to obtain the analytical solution of the vertical structure function, $\gamma = 30$ K and $T_0 = 300$ K are set. Fig. 1(a) and (b) illustrate analytical solutions of the vertical structure functions of $m = 0-5$ and $m = 11-16$ by Terasaki and Tanaka (2007). The sinusoidal solutions are normalized by density stratification of $\sigma^{-\frac{1}{2}}$ and contained in that envelopes. Dividing them into the barotropic mode ($m = 0$) and the baroclinic modes ($m \geq 1$), the former is a function that has no nodes in the vertical direction and the latter have greater amplitudes as going up into the upper atmosphere. We set ϵ at 0.01 hPa, which corresponds to 85.9 km for the standard atmosphere in this study. Refer to Terasaki and Tanaka (2007) for the detail of the analytical vertical structure functions.

The 3-D NMF has orthonormality, therefore U can be expand in the wave numbers:

$$U(\lambda,\theta,\sigma,\tau) = \sum_{n=-N}^{N} \sum_{l=0}^{L} \sum_{m=0}^{M} w_{nlm} X_m \Pi_{nlm}(\lambda,\theta,\sigma), \tag{6}$$

where X_m is a scaling matrix

$$X_m = diag\left(\sqrt{gh_m}, \sqrt{gh_m}, gh_m\right), \tag{7}$$

and h_m denotes the equivalent height for m. These wavenumbers are truncated at N, L, and M. $w_{nlm}(\tau)$ is the ex-

(a)
Analytical Vertical Structure Function

(b)
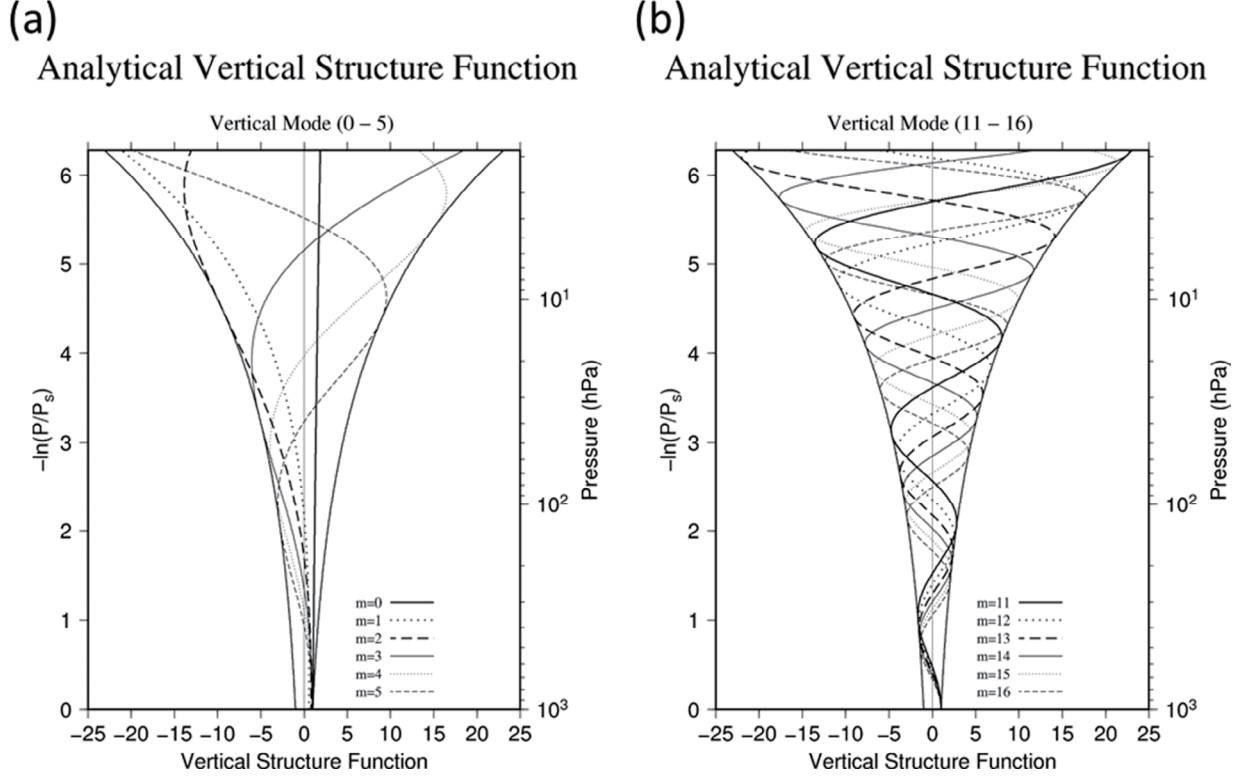### Analytical Vertical Structure Function

Fig. 1 The vertical profiles of the analytical solutions of the vertical structure functions for (a) $m=0$ - 5 and (b) $m=11-16$ from the surface to 1 hPa level (after Terasaki and Tanaka 2007).

pansion coefficients of the state variables of U.

In this study, in order to express AGWs generated in the thermosphere, the temperature departure T is calculated from geopotential field. The temperature departure may be represented from an equation of state and a hydrostatic equation:

$$T = -\frac{\sigma}{R}\frac{\partial \phi}{\partial \sigma}$$

$$= -\frac{\sigma}{R}\sum_{n=-N}^{N}\sum_{l=0}^{L}\sum_{m=0}^{M}w_{nlm}gh_m Z_{nlm}\frac{\partial G_m}{\partial \sigma}e^{in\lambda} \quad (8)$$

where R is a gas constant (= 287.04 [JK^{-1}kg^{-1}]), Z_{nlm} is a geopotential component of Hough functions.

In this study, zonally symmetric initial conditions are considered in reference to the thermal impact of auroral oval, and the meteorological variables are expanded in wavenumbers as $n = 0$, $1 = 1 - 78$ (Rossby mode, west gravity mode and east gravity mode, each 26), $m = 0 - 59$. Note that grid intervals are the 60 Gaussian latitudes and the 960 vertical levels.

An initial value is given by cosine curves with one wavelength in meridional and vertical directions as follows:

$$val = A\left[\cos\frac{(\theta - \theta_0)}{L_y}\pi + 1\right]\left[\cos\frac{(H - H_0)}{L_z}\pi + 1\right] \quad (9)$$

where val is an arbitrary variable of (u, v, ϕ, T), A is an amplitude, θ is latitude, H is height (km), θ_0 and H_0 are the latitude and the height in the initial time, and L_y and L_z are the widths in vertical and meridional directions, respectively.

The $w_{nlm}(0)$ at $t=0$ is determined by Fourier expansion of the variables. The analytical solution of $w_{nlm}(\tau)$ at $t=\tau$ is calculated by $w_{nlm}(\tau)=w_{nlm}(0)e^{-i\sigma_{nlm}\tau}$. The summation of Fourier series provides the meridional and height structure of the variables at any time of the future. In this study, the time integration is performed from the initial time 0 to 24 hours at every 30 minutes. The time change of val is presented in latitude-altitude cross section. The initial value is normalized to have a maximum amplitude 1 since the model is linear although an arbitrary large amplitude is given for drawing purpose. Therefore, the property of propagation of waves is evaluated in terms of the ratio to the initial amplitude of the waves.

Fig. 2 shows the vertical structure of the initial wave with $H_0=15.0$ and $L_z=7.5$ in Eq. (9). The vertical structure are 0 in the outer side of $H_0\pm 7.5km$ because the peak
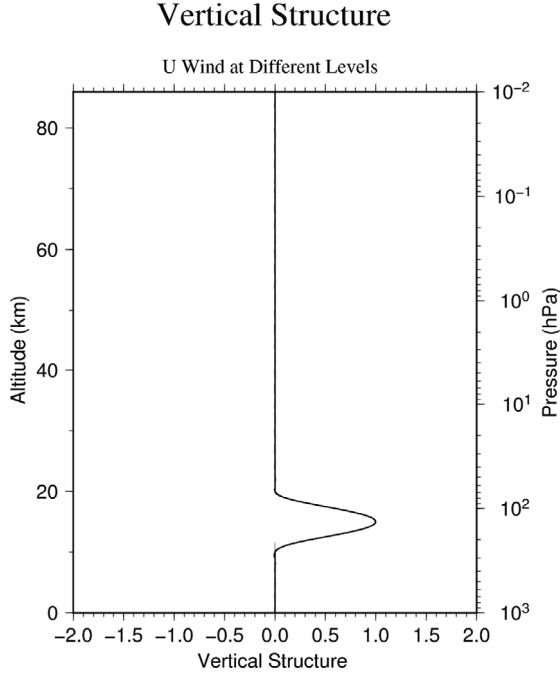
Vertical Structure

U Wind at Different Levels

Fig. 2 A sample of the vertical profile of the initial state of cosine wave for a case of $H_0 = 15.0$ and $L_z = 7.5$.

Time Integration of the Impact
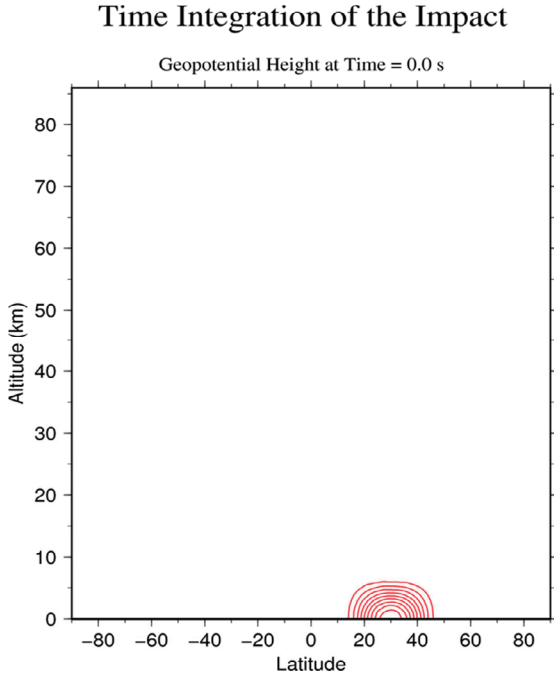
Geopotential Height at Time = 0.0 s

Fig. 3 Latitude-latitude cross section of the geopotential height ϕ in initial time as centered at 30°N and 0 km. The vertical axis indicates altitude (km).

of it is H_0. This sample structure was used for the study of geostrophic adjustment of subtropical jet by the propagation of AGWs (Tanaka and Hagiwara, 2019). In this study, the initial cosine impulse is set at various locations and finally at the top of the model atmosphere as will be described in the next.

3. Results

3.1. Topographic forcing experiment

a. Analysis of vertical wave propagations

As the first experiment, the geopotential height at 30°N on the surface is calculated to examine AGWs propagating from the surface to the upper atmosphere. The wave source is located at 0 km as cosine waves with widths 7.5 km in vertical direction centered at 30°N with 20°N width; val = ϕ, $A = 0.25$, $\theta = 30$, $L_y = 20$, $H_0 = 0$, $L_z = 7.5$. Note that no zonal wind u, and meridional wind v is given for the initial state. For the sake of drawing, the maximum value at initial time is set to 0.25 m in this analysis.

Fig.3 shows the latitude-height section of geopotential height at $t = 0$. The time integration from the initial state is performed for arbitrary time. Fig. 4 illustrates geopotential every 6 hours after the initial showing both positive and negative geopotential heights. The wave spreads symmetrically around 30°N. The waves at the mid-latitudes in the initial state reach the high altitudes and propagate horizontally. The vertical propagation of group velocity is upward, and the phase speed is downward, perpendicular to the group velocity. Those correspond to the linear theory of AGWs as described in Holton (1979). The top altitude in these figures is the top of the model atmosphere to solve the vertical structure function. The waves are reflected at the boundaries because analytical solutions used in this study are linear solutions without the nonlinearity and forcing term. Fig. 5 shows the result of geostrophic adjustment at t → ∞, extracting only the geostrophic mode setting 0 for AGWs. Only the geostrophic mode remains after the geostrophic adjustment. The AGWs are not attenuated by the analytical solution. Yet, we have assumed here that the AGWs will dissipate at t → ∞. The positive geopotential height with initial semicircular structure is present although slightly deformed, and the negative geopotential height appears aloft.

3.2. Subtropical jet experiment

a. Analysis of geostrophic adjustment

As the second experiment, the geopotential height at 30°N and 15 km height is calculated to examine AGWs propagating from the subtropical jet to the all directions ; val = ϕ, $A = 0.25$, $\theta_0 = 30$, $L_y = 20$, $H_0 = 15$, $L_z = 7.5$. Note that no zonal wind u, and meridional wind v is given for the initial state.

Fig.6 shows the latitude-height section of geopotential height at $t = 0$. The time integration from the initial state is performed for arbitrary time. Fig. 7 illustrates geopotential height 12 hours after the initial, showing both positive and negative geopotential heights, and the wave
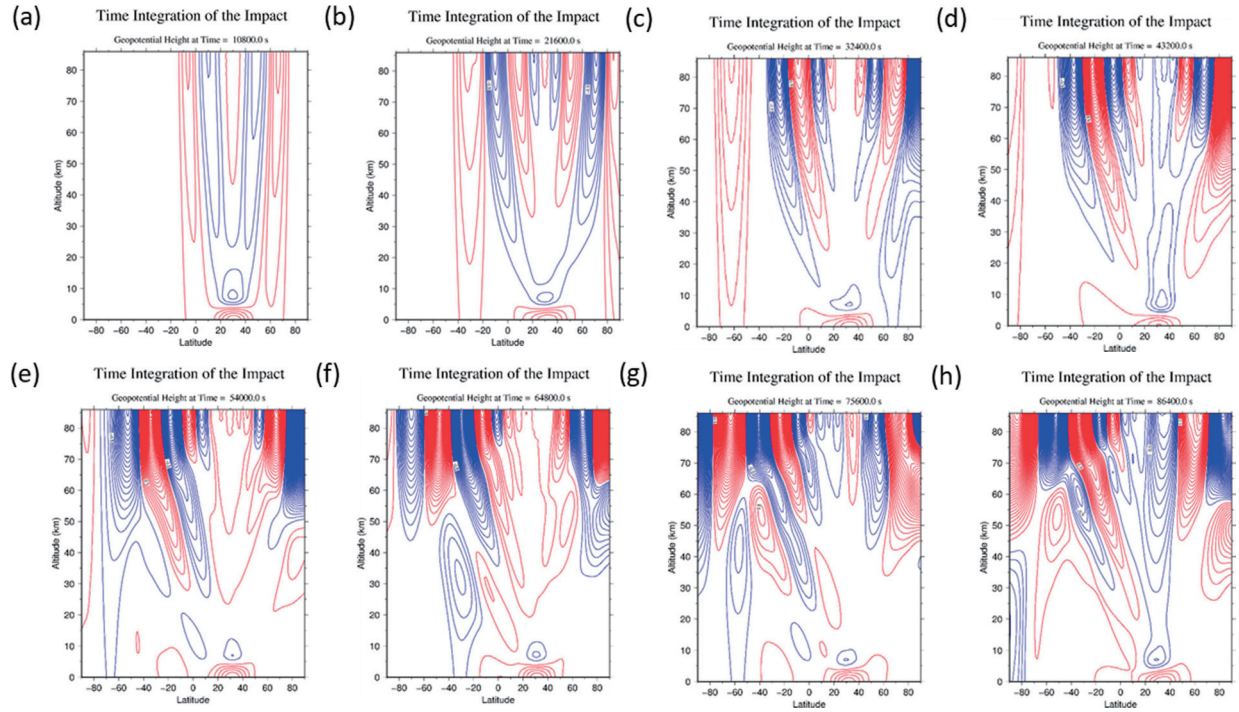
Fig. 4 Latitude-latitude cross section of the geopotential height ϕ the same as Fig. 3, but after (a) 3 hours, (b) 6 hours, (c) 9 hours, (d) 12 hours, (e) 15 hours, (f) 18 hours, (g) 21 hours, and (h) 24 hours.
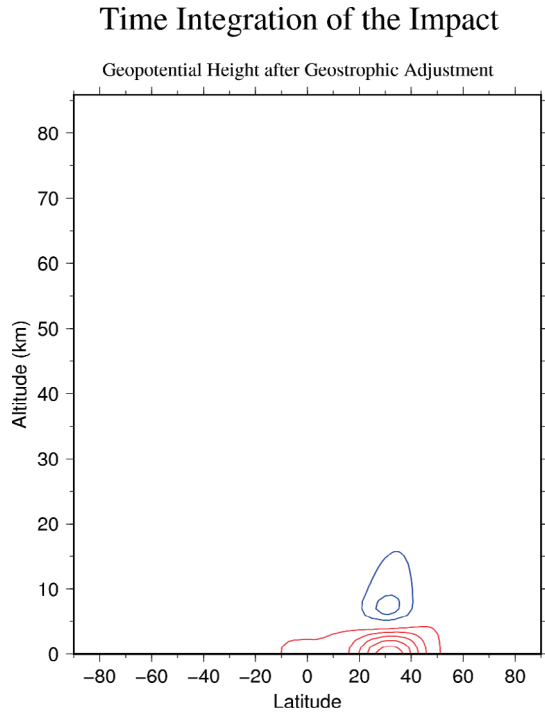

Fig. 5 Latitude-latitude cross section of the geopotential height ϕ the same as Fig. 3, but after the geostrophic adjustment.
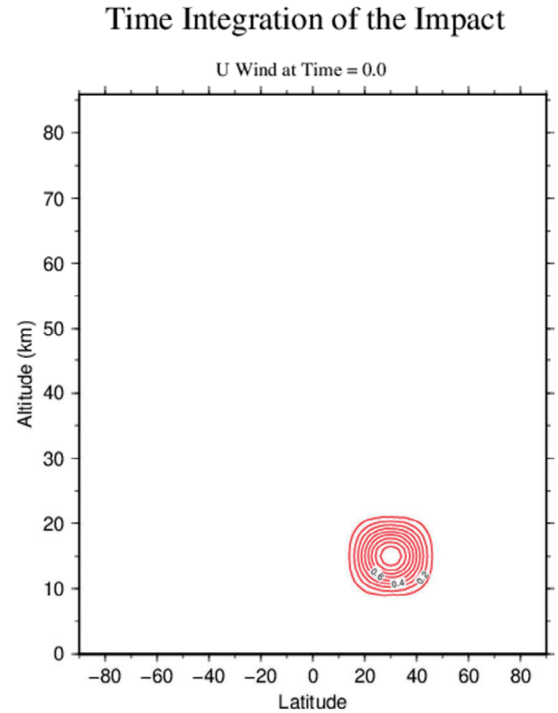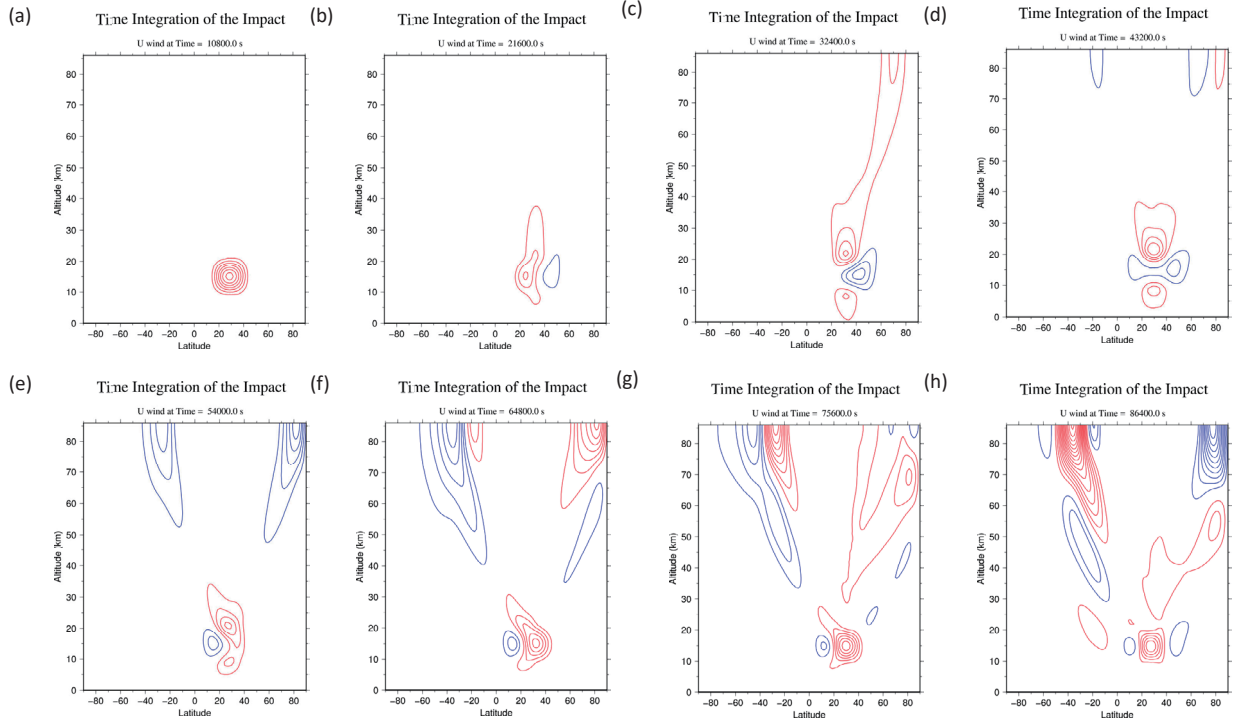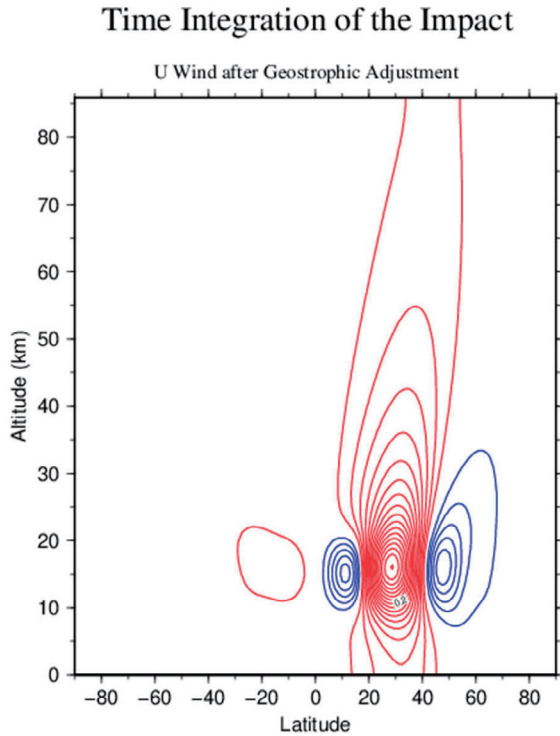
Fig. 6 Latitude-latitude cross section of the geopotential height ϕ in initial time as centered at 30°N and 15 km. The vertical axis indicates altitude (km).

Fig. 7 Latitude-latitude cross section of the geopotential height ϕ the same as Fig. 6, but after (a) 3 hours, (b) 6 hours, (c) 9 hours, (d) 12 hours, (e) 15 hours, (f) 18 hours, (g) 21 hours, and (h) 24 hours.

Fig. 8 Latitude-latitude cross section of the geopotential height ϕ the same as Fig. 6, but after the geostrophic adjustment.
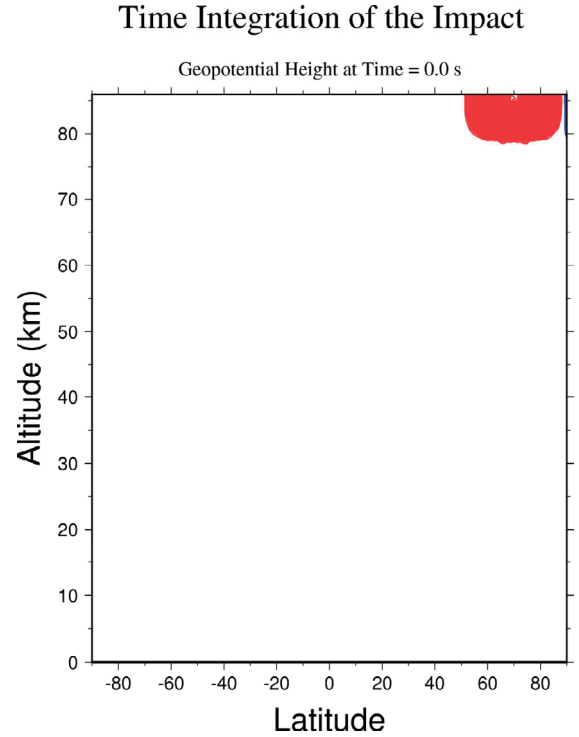

Fig. 9 Latitude-height cross section of geopotential ϕ in initial time as centered at 70°N and 85.9 km. The values are normalized by the density stratification $\sigma^{\frac{1}{2}}$. The contours show geopotential height at 2.0 m intervals. The red lines are positive values and the blue lines are negative values.
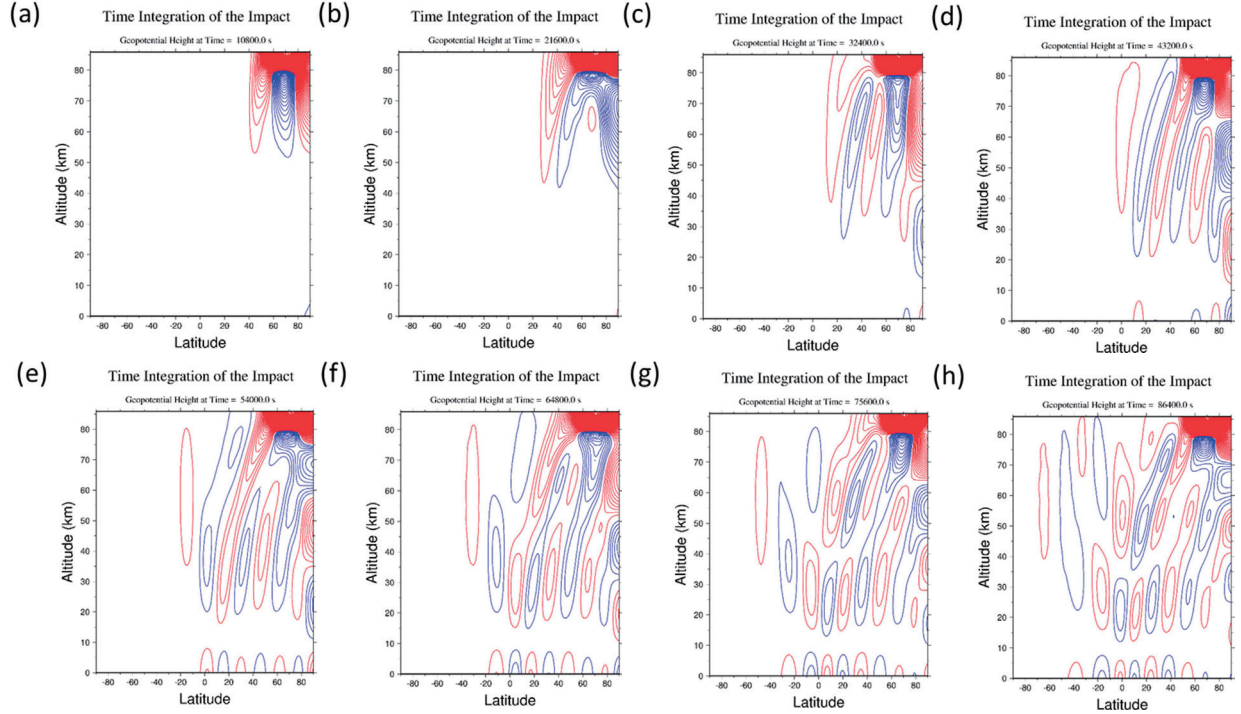
7

Fig. 10 Latitude-height cross section of geopotential ϕ as in Fig. 9, but after (a) 3 hours, (b) 6 hours, (c) 9 hours, (d) 12 hours, (e) 15 hours, (f) 18 hours, (g) 21 hours, and (h) 24 hours.

spreads symmetrically around 30°N. The waves at the mid-latitudes in the initial state reach the high altitudes and propagate horizontally. The vertical propagation of group velocity is upward, and the phase speed is downward, perpendicular to the group velocity. Fig. 8 shows the result of geostrophic adjustment at t → ∞, extracting only the geostrophic mode setting 0 for AGWs. The positive geopotential height with initial circular structure is present although slightly deformed, and the negative geopotential height appears at high and low latitudes.

3.3. Aurora oval experiments

a. Analysis at high latitudes and high altitude

As the third experiment, the geopotential height at 70°N of top boundary is calculated to examine AGWs propagating downward from the thermosphere to the troposphere. The wave source is located at 85.9 km as cosine waves with widths of 7.5 km centered at 70°N of 20°N width ; $val = \phi$, $A = 25000$, $\theta_0 = 70$, $L_y = 20$, $H_0 = 85.9$, $L_z = 7.5$. Note that no zonal wind u, and meridional wind v is given for the initial state.

Fig.9 shows the latitude-height section of geopotential height at t = 0. This represents auroral oval occurring at high latitudes. In the following figures, the geopotential height is normalized by the density stratification of $\sigma^{-\frac{1}{2}}$ to express the behavior of the waves of small amplitude.
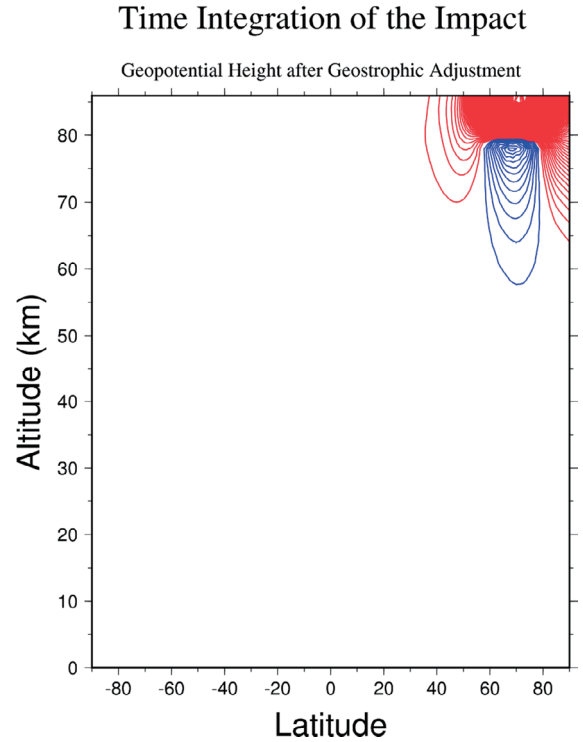

Fig. 11 Latitude-height cross section of geopotential ϕ as in Fig. 9, but after geostrophic adjustment at $t \rightarrow \infty$.
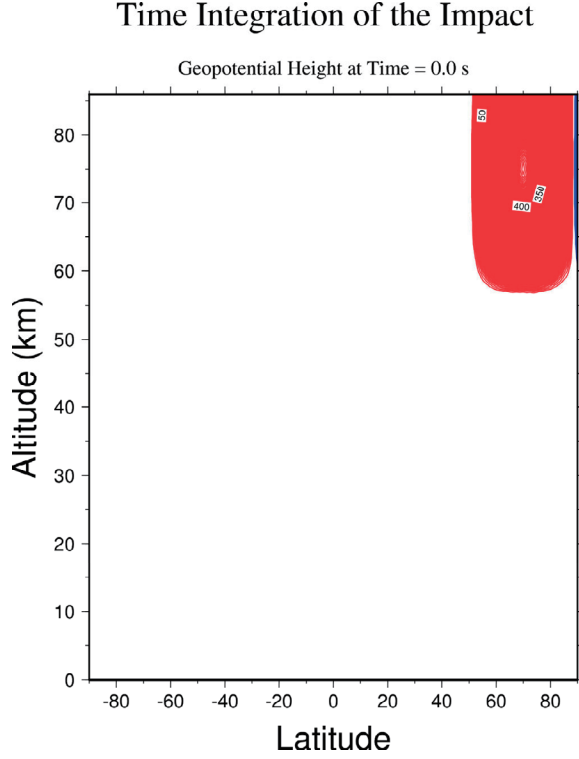
8

Time Integration of the Impact

Fig. 12 Latitude-height cross section of geopotential ϕ as in Fig. 9, but with the vertical width of 30 km.

The time integration from the initial state is performed up to 24 hours. Fig. 10(a) – (h) illustrates that both positive and negative geopotential heights appear at 60 – 80 km altitude, and the waves propagating downward. The vertical propagation of waves is remarkable in the Arctic for 9 hours after the initial impact (Fig.10 (c) – (h)). The wave energy from high altitudes propagates downward; the group velocity goes diagonally downward and the phase velocity propagates upward at right angles to it. The waves are reflected at the boundaries because analytical solutions used in this study are linear solutions without the nonlinearity and forcing term. In addition, standing waves are formed from the surface to 7.5 km altitudes in mid/low latitudes after 12 hours. The surface amplitude of waves is about 1/10,000 by 24 hours compared to the initial state. Fig. 11 shows the result of geostrophic adjustment at $t \rightarrow \infty$, extracting only the geostrophic mode setting 0 for AGWs. The geostrophic adjustment shows only the geostrophic modes. The positive geopotential height with initial semicircular structure is present although slightly deformed, and the negative geopotential height arises at 60 - 80 km.

b. Analysis with different vertical width

In order to examine how the wave propagates by changing the wave source, an analysis is performed in
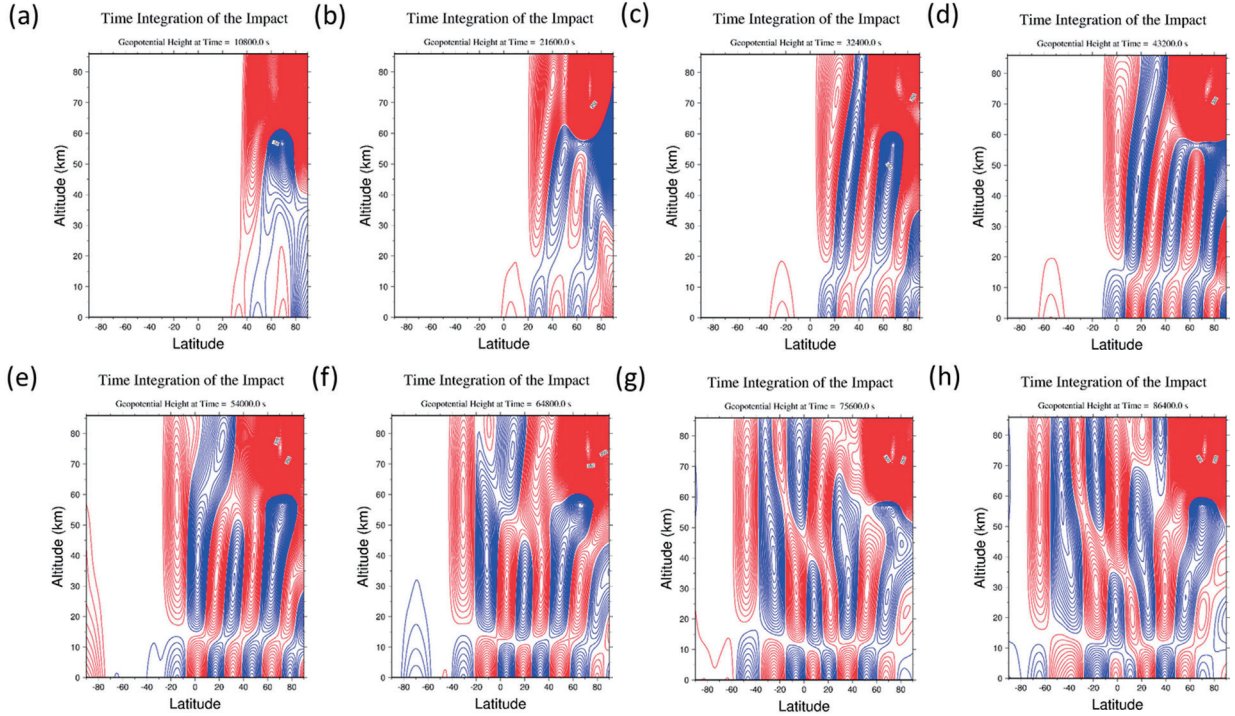

Fig. 13 Latitude-height cross section of geopotential ϕ as in Fig. 12, but after (a) 3 hours, (b) 6 hours, (c) 9 hours, (d) 12 hours, (e) 15 hours, (f) 18 hours, (g) 21 hours, and (h) 24 hours.

Misako HAGIWARA and Hiroshi L. TANAKA

Time Integration of the Impact

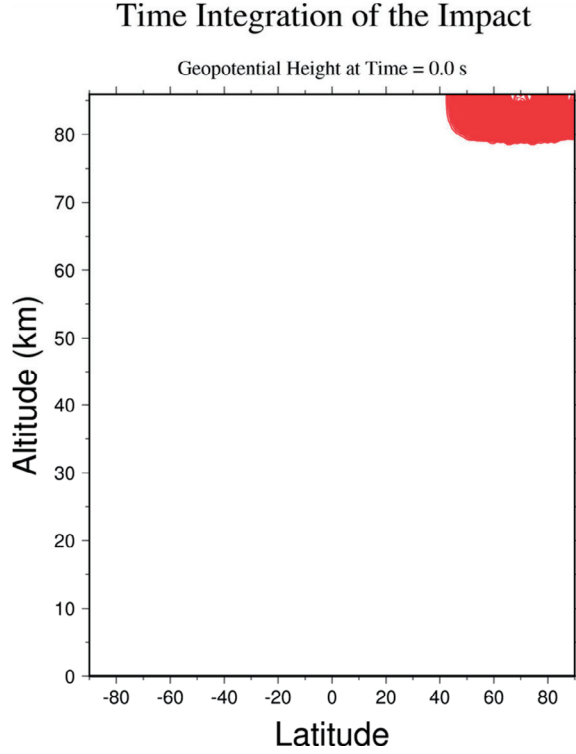### Geopotential Height at Time = 0.0 s

Fig. 14 Latitude-height cross section of geopotential ϕ as in Fig. 9, but with the horizontal width of 30 degrees.

which the horizontal and vertical widths of the geopotential height at initial state are altered. At the same location, geopotential height is set as a cosine wave with widths of 20 degrees in horizontal direction and 30 km in vertical direction; $val = \phi$, $A = 25000$, $\theta_0 = 70$, $L_y = 20$, $H_0 = 85.9$, $L_z = 30.0$. In Fig. 12 at $t = 0$, positive geopotential height is formed above 55 km. The propagation of this wave source is shown in Fig. 13. Compared to Fig. 10, the wave reaches the surface 3 hours later, the response to the impact on the troposphere is larger. After 12 hours (Fig. 13 (d)), the wave reaches the equatorial troposphere. As in Fig. 10, standing waves with nodes at 15 km are formed. The amplitude in the initial state decreases by about 2,000 times by 24 hours.

c. Analysis with different horizontal width

Moreover, an analysis with different horizontal width is performed; $val = \phi$, $A = 25000$, $\theta_0 = 70$, $L_y = 30$, $H_0 = 85.9$, $L_z = 7.5$. In the initial state (Fig. 14), positive geopotential heights with a vertical width of about 7.5 km are formed horizontally from the North Pole to latitude 40°N. Fig. 15 shows this propagation of waves as similar to Fig. 10. The meridional scale of propagating waves is common despite the different meridional scale of the initial impact. However, it is found that the amplitude of waves is extremely smaller than that in Fig. 10.
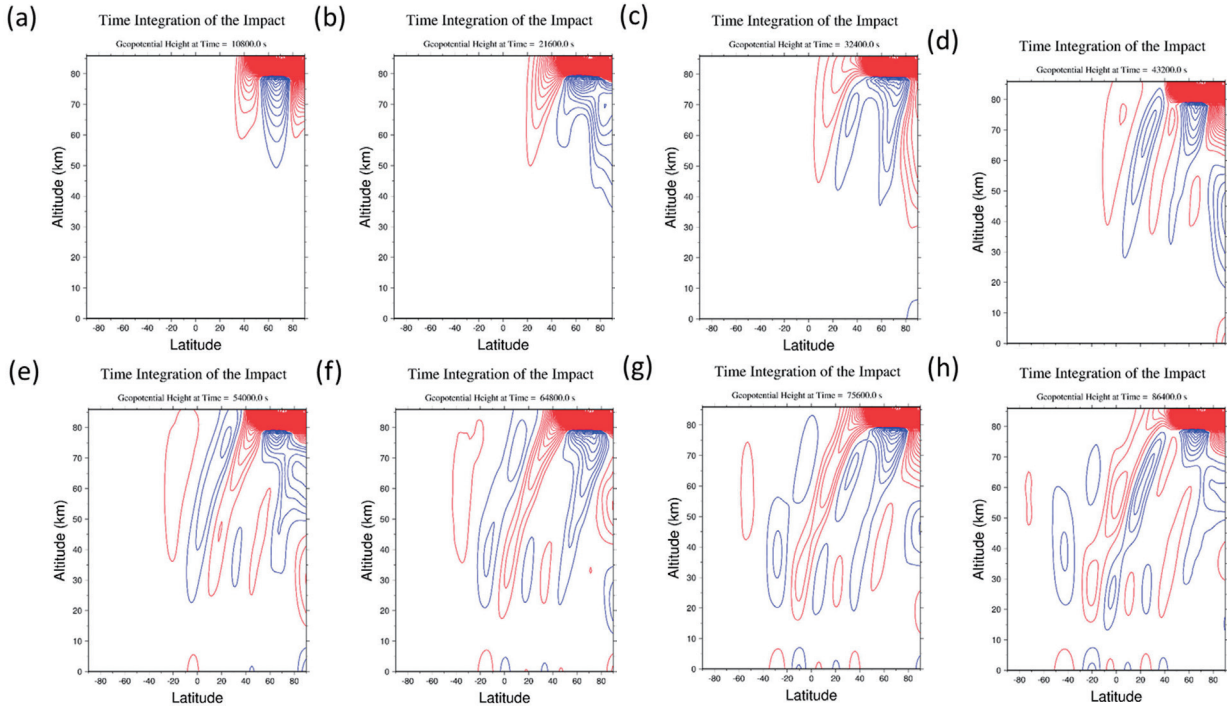

Fig. 15 Latitude-height cross section of geopotential ϕ as in Fig. 14, but after (a) 3 hours, (b) 6 hours, (c) 9 hours, (d) 12 hours, (e) 15 hours, (f) 18 hours, (g) 21 hours, and (h) 24 hours.
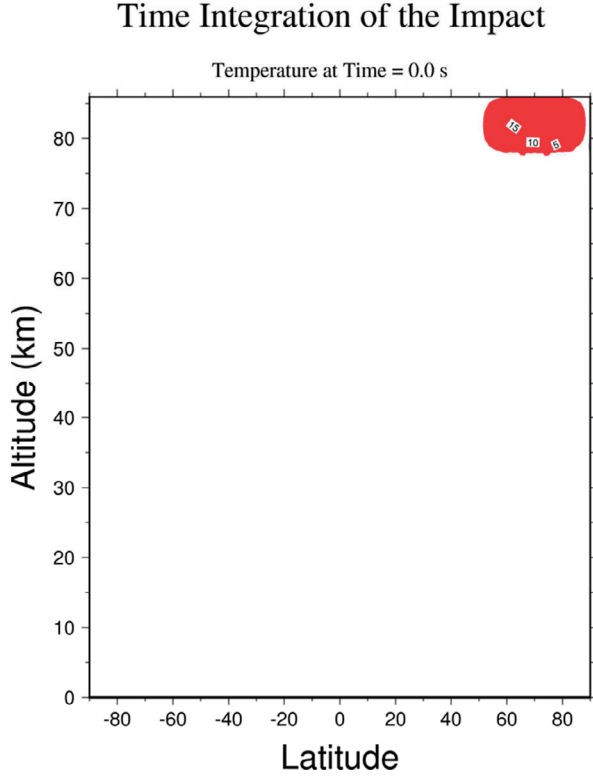
Time Integration of the Impact

Fig. 16 Latitude-height cross section of temperature T at initial time centered at 70°N and 85.9 km. The values are normalized by the density stratification $\sigma^{-\frac{1}{2}}$. The contours show temperature interval at 0.01 K. The red lines are positive values and the blue lines are negative values.

3.4. Temperature waves

a. Analysis at high latitudes and altitude

The temperature departure is described as is the case of 3.3. First, Fig. 16 shows the wave source as in Fig. 9; $val = T$, $A = 25000$, $\theta_0 = 70$, $L_y = 20$, $H_0 = 85.9$, $L_z = 7.5$. In Fig. 16, the positive temperature departure with the initial ellipsoidal structure seen. In Fig. 17, the positive area is divided into both north and south at 70°N, and propagates horizontally and vertically. The waves reaching North Pole are reflected back to low latitude, where vertical propagation is more predominant than horizontal propagation. The propagating waves reach the equatorial troposphere after 18 hours. Fig.17 (f) – (h) shows that the waves diagonally propagate to 30 km. Standing waves at the surface as seen in Fig. 10 are formed, whose nodes is formed at the surface. It is quantitatively assessed that the amplitude propagating to the troposphere is about 1/15,000 by 24 hours. The result of geostrophic adjustment is shown in Fig. 18. This obtains only geostrophic modes, and negative departures exist at 60 – 80 km.
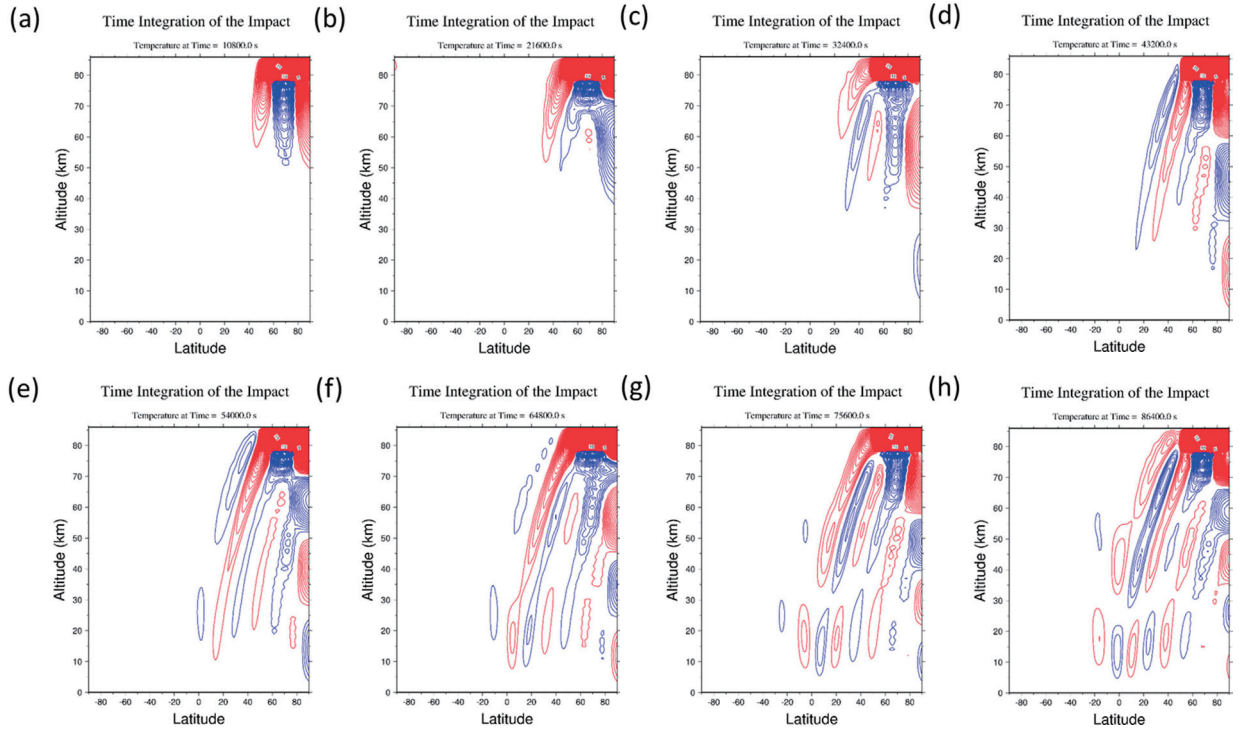

Fig. 17   Latitude-height cross section of temperature T as in Fig. 16, but after (a) 3 hours, (b) 6 hours, (c) 9 hours, (d) 12 hours, (e) 15 hours, (f) 18 hours, (g) 21 hours, and (h) 24 hours.
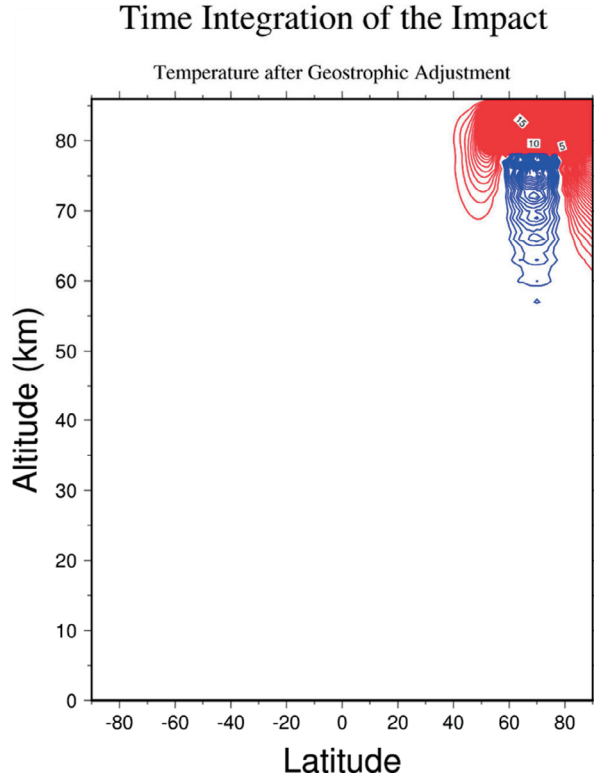
11

Time Integration of the Impact

Fig. 18 Latitude-height cross section of temperature T as in Fig. 16, but after geostrophic wind adjustment at $t \rightarrow \infty$.

4. Summary and discussion

In this study, downward vertical propagation of AGWs generated in thermosphere is examined using 3-D NMF. The propagation of the waves is analytically expressed as a function of time.

First, we conducted an experiment at 30°N, and found that the waves propagate symmetrically around 30°N at the geopotential altitude, and that the directions of group and phase velocities of the propagating waves are mutually orthogonal. Since the altitude at the top of the figure is the top of the atmosphere itself int the model, the waves are reflected at this altitude, which is used to solve the vertical structure function. Since the altitude at the top of the figure is the top of the atmosphere itself, the waves are reflected at this altitude, which is used to solve the vertical structure function. The analytical solution used in this study is a linear solution without nonlinear terms and external forcing terms, so the reflection of the theoretical waves is represented here. The wave sources of the sub-tropical jet increase in amplitude to the upper latitudes, and both westerly and easterly winds strengthen with time.

Under the assumption of thermal impact by aurora oval, propagation characteristics in the geopotential height and temperature are investigated. The group veloc-ity of AGWs travels diagonally downward from the wave source to the surface, indicating the upward phase velocity.

With respect to AGWs in geopotential height, anti-nodes of standing waves are formed at the surface. This result suggests that both waves from upper atmosphere and waves reflected at the surface interfere with each other. In the analysis with a longer vertical width of the wave source, the nodes of standing wave are formed at higher altitudes, responding to the different vertical width of the initial state. The nodal structure may be the result from the lower boundary condition of the vertical structure function. On the other hand, temperature departure indicates a nodal structure of the standing waves at the surface. For the wider vertical width, more energy is contained in the middle atmosphere at $t = 0$. The vertical width of propagating AGWs becomes wider, and reaches the troposphere in a short time. The amplitude of AGWs is quantitatively estimated to decrease by one six hundredth. This result is about 25 times larger than that of default horizontal width of 20 degrees and vertical width 7.5 km. In the case of vertical width 15 km, which is not mentioned in this paper, the amplitude is about 5 times larger. Therefore, there is proportional relationship between the vertical width and the amplitude of the wave. Compared to the geopotential height, it is found that the larger the vertical width, the greater the temperature response. In the analysis with the longer meridional width of the wave source, the width of propagating AGWs is not altered by the different meridional scale of the impact. Although the amplitude of AGWs becomes smaller, the damping rates of it in the geopotential height and the temperature departure are equivalent. Therefore, propagating wave structures depend mostly on their vertical widths of the initial impact.

Standing waves formed by propagation of waves in temperature departure have anti-nodes at 10 km. Vertical derivative of temperature is equivalent to temperature lapse rate and stability parameter. Therefore, negative (positive) vertical derivative at 10 km becomes unstable (stable) stratification. This means that it can trigger the development of cyclones because stability in the troposphere is changed in synoptic-scale disturbance as suggested by Prikryl et al. (2016; 2018).

The temperature increase by the auroral oval is estimated as hundreds to a thousand K (400 K, personal communication by Dr. S.I. Akasofu). Assuming that there is no damping in downward propagation of AGWs, the amplitude of AGWs has been reduced from 1,000 to 10,000 times. The result shows that the temperature departure reaching the surface becomes about 0.01 – 0.1 K. Although the magnitude is quite small, the same amount

of response could persist for several days of magnetic storms, or for 1000 years in the long-term variation of solar activities. However, it is left as a future subject because these impacts on the troposphere are not observed.

In this study, theoretical AGWs are expressed by solving a linear theory using the expansion in 3-D NMF. In 3-D NMF, the static stability parameter γ is assumed as constant, which allows the analytical vertical function. However, γ changes in the real atmosphere above stratosphere. It is needed to consider the vertical change of γ to apply for real atmosphere. In addition, this analysis doesn't include effects on friction, viscosity, and radiative cooling. The amplitudes of AGWs reaching the troposphere may drop to thousands times smaller in a real atmosphere.

On the other hand, solar activity, atmospheric composition, and aurora activity cause large temperature changes in the thermosphere, which sometimes results in a difference of several hundred degrees in terms of daily change. Moreover, the damping rate is an important parameter to understand the momentum dissipation process during wave propagation from high to middle or low latitudes (Oyama and Watkins, 2012). The analysis including effects on friction, viscosity, and radiation is needed to describe more real atmosphere.

Acknowledgments

References

Chimonas, G. and C. O. Hines (1970): Atmospheric gravity waves launched by auroral currents, *Planet. Space Sci.*, **18**, 565-582.

Crowley, G. and P. J. S. Williams (1987): Observations of the source and propagation of atmospheric gravity waves, *Nature*, **328**, 231-233.

Francis, S. H. (1974): A theory of medium-scale traveling ionospheric disturbances. *J. Geophys. Res.*, **79**, 5245-5260.

Francis, S. H. (1975): Global propagation of atmospheric gravity waves: A review. *J. Atmos. Terr. Phys.*, **37**, 1011-1054.

Fujita, R. and H. L. Tanaka (2007): Statistical analysis on the relationship between solar and geomagnetic activities and the Arctic Oscillation. *J. Meteor. Soc. Japan*, **85**, 909-918.

Gray, L. J., J. Beer, M. Geller, J. D. Haigh, M. Lockwood, K. Matthes, U. Cubasch, D. Fleitmann, G. Harrison, L. Hood, J. Luterbacher, G. A. Meehl, D. Shindell, B. van Geel, and W. White (2010): Solar influences on climate. *Rev. Geophys.*, **48**, RG4001, doi:10.1029/2009RG000282.

Holton, J. R. (1979): An introduction to dynamic meteorology. *Academic Press.*, **23**, 391pp.

Idenden, D. W. (1998): The thermospheric effects of a rapid polar cap expansion. *Ann. Geophysicae*, **16**(10), 1380-1391.

Kamae, Y., T. Kawana, M. Oshiro, and H. Ueda (2017): Seasonal modulation of the Asian summer monsoon between the Medieval Warm Period and Little Ice Age: a multi model study. *Prog. Earth Planet. Sci.*, **4**, 22.

Kodera, K. and Y. Kuroda (2002): Dynamical response to the solar cycle. *J. Geophys. Res.*, **107**(D24), 4749, doi:10.1029/2002JD002224.

Kristjánsson, J. E., A. Staple, J. Kristiansen, and E. Kaas (2002): A new look at possible connections between solar activity, clouds and climate. *Geophys. Res. Lett.*, **29**(23), 2107, doi:10.1029/2002GL015646.

Matsuno, T. (1982): A quasi one-dimensional model of the middle atmosphere circulation interacting with internal gravity waves. *J. Meteor. Soc. Japan*, **60**, 215-226.

Mayr, H. G., I. Harris, F. A. Herrero, N. W. Spencer, F. Varosi, and W. D. Pesnell (1990): Thermospheric gravity waves: Observations and interpretation using the transfer function model. *Space Sci. Rev.*, **54**, 297-375.

Mayr, H. G., E. R. Talaat, and B. C. Wolven (2013): Global propagation of gravity waves generated with the whole atmosphere transfer function model. *J. Atmos. Sol. Terr. Phys.*, **104**, 7-17.

Ney, E. P. (1959): Cosmic radiation and the weather. *Nature*, **183**, 451-452.

Ogura, Y. (1997): Basic theory of meso-scale meteorology. *University of Tokyo Press.*, Tokyo, 215pp (in Japanese).

Oyama, S., and B. J. Watkins (2011): Generation of atmospheric gravity waves in the polar thermosphere in response to auroral activity, *Space Science Reviews*, **168**(1-4), 463-473, doi:10.1007/s11214-011-9847-z.

Pierce, J. R., and P. J. Adams (2009): Can cosmic rays affect cloud condensation nuclei by altering new particle formation rates? *Geophys. Res. Lett.*, **36**, L09820, doi:10.1029/2009GL037946.

Prikryl, P., D. B. Muldrew, and G. J. Sofko (2003): High-speed solar wind, auroral electrojets and atmospheric gravity waves: A link to the Earth's atmosphere, in Proceedings of the ISCS 2003 Symposium: Solar

Variability as an Input to the Earth's Environment, Tatranska Lomnica, ESA SP-535, 371-376.

Prikryl, P., K. Iwao, D. B. Muldrew, V. Rušin, M. Rybanský, and R. Bruntz (2016): A link between high-speed solar wind streams and explosive extratropical cyclones. *J. Atmos. Sol. Terr. Phys.*, **149**, 219-231.

Prikryl, P., R. Bruntz, T. Tsukijihara, K. Iwao, D. B. Muldrew, V. Rušin, M. Rybanský, M. Turňa, and P. Šťastný (2018): Tropospheric weather influenced by solar wind through atmospheric vertical coupling downward control. *J. Atmos. Sol. Terr. Phys.* **171**, 94-110.

Richmond, A. D. and S. Matsushita (1975): Thermospheric response to a magnetic substorm. *J. Geophys. Res.*, **80**(19), 2839-2850.

Richmond, A. D. (1978): Gravity wave generation, propagation, and dissipation in the thermosphere, *J. Geophys. Res.*, **83**, 4131-4145.

Sato, K., R. Yasui, and Y. Miyoshi (2018): The momentum budget in the stratosphere, mesosphere, and lower thermosphere. Part I: Contributions of different wave types and in situ generation of Rossby waves, *J. Atmos. Sci.*, **75**, 3613-3633, doi:10.1175/JASD-17-0336.1.

Svensmark, H., and E. Friis-Christensen (1997): Variations of cosmic ray flux and global cloud coverage? — a missing link in solar-climate relationships. *J. Atmos. Terr. Phys.*, **59**, 1225-1232, doi:10.1016/S1364-6826(97)00001-1.

Tanaka, H. L. (1985): Global energetics analysis by expansion into three dimensional normal mode functions during the FGEE winter. *J. Meteor. Soc. Japan*, **42**, 950-960.

Tanaka, H. L. and M. Hagiwara (2019): Geostrophic adjustment of subtropical jet on a sphere by the analytical solution. Abstract in Fall Meeting of Meteor. Soc. Japan (in Japanese).

Tanaka, T. (1979): Global structure and dynamics of the thermo-ionospheres, *Rev. Radio Res. Labs.*, **25**(134), 265-309 (in Japanese).

Terasaki, K. and H.L. Tanaka (2007): An analysis of the 3D atmospheric energy spectra and interactions using analytical vertical structure functions and two re-analyses. *J. Meteor. Soc. Japan*, **85**, 785-796.

Tsuda, T. (2011): Characteristics of atmospheric gravity waves observed with the MU (Middle and Upper atmosphere) radar and GPS radio, *Nagare*, **30**(5), 377-384.

Tsuda, T. (2014): Characteristics of atmospheric gravity waves observed using the MU (Middle and Upper atmosphere) radar and GPS (Global Positioning System) radio occultation, *Proc Jpn Acad Ser B Phys Biol Sci.*, **90**(1),12-27, doi:10.2183/pjab.90.12

Vadas, S. L., D. C. Fritts, and M. J. Alexander (2003): Mechanism for the generation of secondary waves in wave breaking regions. *J. Atmos. Sci.*, **60**, 194-214.

Wilcox, J. M., P. H. Scherrer, L. Svalgaard, W. O. Roberts, and R. H. Olson (1973): Solar magnetic sector structure: Relation to circulation of the earth's atmosphere. *Science*, **180**, 185-186.

Xu, J., A. K. Smith, W. Wang, G. Jiang, W. Yuan, H. Gao, J. Yue, B. Funke, M. López-Puertas, and J. M. Russell III (2013): An observational and theoretical study of the longitudinal variation in neutral temperature induced by aurora heating in the lower thermosphere. *J. Geophys. Res. Space Physics*, **118**, 7410-7425, doi:10.1002/2013JA019144.

Yasui, R., K. Sato, and Y. Miyoshi (2018): The momentum budget in the stratosphere, mesosphere, and lower thermosphere. Part II: The in situ generation of gravity waves. *J. Atmos. Sci.*, **75**, 3635-3651, doi:10.1175/JAS-D-17-0337.1.